Materials Advances

PAPER

Check for updates

Gas sensing properties of a Cu-doped PANI nanocomposite towards ammonia

Arunima Verma and Tanuj Kumar [iD] *

This study exhibits the use of nanocomposite films containing copper nanoparticles at various concentrations to selectively detect ammonia gas. Using the chemical oxidative polymerization method, the samples were submerged in a PANI matrix and then subjected to varying concentrations of NH_3 at room temperature to investigate their gas-sensing capabilities. For 100 ppm of NH_3 gas, a gas sensing response of 51% was achieved for PANI loaded with 0.2 g of Cu nanoparticles (PANI@Cu1). Combining PANI@Cu with nanocomposite porosity augmentation improves the resistance, which was already robust before NH_3 deprotonation. An extraordinarily high level of selectivity towards NH_3 gas at ambient temperature was seen in films with a 2 g loading of Cu embedded in a PANI matrix (PANI@Cu5), among the many compositions that were tested. With a recovery time of less than 20 seconds, the resultant sensor responded with 62% accuracy at 300 ppm. Aside from NH_3 gas, the designed sensor is less selective for ethanol, CO, CO_2, and H_2S.

1. Introduction

Ammonia (NH_3) is a major polluting gas that has substantial consequences for human health. It exists in industries such as the chemical industry, agriculture, coal, and manufacturing, and its concentration requires precise monitoring.[1] Recently, ammonia has been identified as a biomarker in exhaled gas. Exhaled gas with a high proportion of NH_3 is thought to be an indicator of kidney illness.[2,3] The Occupational Safety and Health Administration of the United States has issued several ammonia-related warnings. Eight hours at 25 ppm and fifteen minutes at 35 ppm are considered safe levels of ammonia for humans to be exposed to. Serious health concerns, and even death, can result from prolonged exposure and inhalation of it at concentrations greater than 5000 ppm.[4] Therefore, it is extremely desired and crucial to build a low concentration ammonia monitoring system in addition to preventing ammonia leakage. Several metal oxide semiconductors, including $Cu_2O–MoS_2$, SnO_2, In_2O_3 and so on, have been utilised by researchers as ammonia sensors thus far.[5–7] High temperatures, usually between 200 and 500 °C, are optimal for the operation of sensors based on metal oxide semiconductors. Power consumption would be significant due to a high operating temperature, which would limit their usefulness in many areas. Since then, there has been a flurry of activity among scientists working to perfect gas sensors that can detect gases at ambient temperature. Polyaniline (PANI) was singled out as a promising choice among conductive polymers due to its many advantageous characteristics, including its inexpensive cost, ease of production, distinctive electrical and redox characteristics, rapid response time, and ability to operate at room temperature.[8,9] Doping and de-doping are two common methods for controlling PANI resistance, while varying the degree of protonation with certain additives and target gases alters the material electrical resistivity. It has been demonstrated that the sensing characteristics of PANI composites could be significantly enhanced by the addition of metal.[10]

Our present focus is on developing a sensor by combining a PANI matrix with copper (Cu), an inorganic material. The decision to choose copper as a material was influenced by multiple considerations such as good biocompatibility, lack of toxicity, excellent chemical stability, high electron transfer capability, excellent mechanical strength, and direct wide band gap (E_g = 1.0–1.9 eV).[11,12] The incorporation of copper within the PANI matrix significantly enhances the composite properties, rendering it a promising material for various advanced applications. Copper's excellent electrical conductivity, coupled with PANI's intrinsic conductivity, results in an improvement in the overall conductivity of the composite. Furthermore, the presence of copper imparts superior catalytic activity, making the PANI–Cu composite an attractive candidate for applications in sensors, energy storage devices, and catalysis. The enhanced stability and durability of the composite, attributed to the strong interaction between copper and the PANI matrix, further underscores its potential for practical application. Several studies have examined employing PANI or a PANI–metal nanoparticle combination to improve electrical and optical aspects. For example, Shivam Kumar *et al.*[13] developed a highly sensitive Cu–ethylenediamine/PANI composite film for gas sensing,

Department of Nanoscience & Materials, Central University of Jammu, Jammu, 181143, India. E-mail: tanuj.nsm@cujammu.ac.in

by integrating I and Cu functionalities into the Zr-UiO-67 material, Khalid Mujasam Batoo et al.[14] demonstrated not only enhanced CO uptake capacity but also a significant increase in CO conversion efficiency, as measured by evolution rate, and presented a MOF-based design strategy for achieving high selectivity and productivity in the photocatalytic reduction of CO to MeOH. A novel MXene/TiO$_2$/C-NFs heterojunction-based sensory component for NH$_3$ detection was created by Sagar Sardana et al.,[15] with cellulose nanofibers (C-NFs) serving as the substrate. This sensor is very sensitive to NH$_3$, has a high selectivity, and is very reproducible. For self-powered breathing and environmental monitoring, Sagar Sardana et al.[16] investigated edge-site-enriched Ti$_3$C$_2$T$_x$ MXene/MoS$_2$ nanosheet heterostructures. In addition, Zhang et al.[17] developed a polyaniline/silver nanocomposite for the determination of formaldehyde, and Cui et al.[18] fabricated a polyaniline/titanium dioxide nanocomposite film by layer-by-layer self-assembly, but a lot still remains to be explored. These considerations motivated the chemical polymerization synthesis of copper in a PANI matrix, which formed the basis of a room temperature ammonia sensor. In this study, PANI and its composites were made on a Si substrate using the spin-coating procedure with five different concentrations of copper sources. The nanocomposites were studied with XRD, FTIR, EDX, FE-SEM, UV-Vis absorption spectroscopy and TGA techniques, respectively. The gas-sensing capabilities of the samples were tested by exposing them to varying amounts of NH$_3$ at room temperature. Furthermore, the mechanisms and impacts of copper on sensor behaviour for ammonia detection were thoroughly examined.

2. Experimental details

2.1 Materials and reagents

Ammonium persulfate (APS) (M.W. 228.20 g mol^{-1}, Sigma-Aldrich), copper acetate Cu(OAc$_2$) (M.W. 181.63 g mol^{-1}, Sigma-Aldrich), aniline monomer (M.W. 93.13, AR), and hydrochloric acid (M.W. 36.46 g mol^{-1}, AR) were procured. No additional purification was performed on the other reagents prior use. All of the solutions used in the experiment were prepared using double distilled water.

2.2 Synthesis of polyaniline (PANI)

PANI was synthesized using a method involving the mixing of solutions. Scheme 1 shows the use of ammonium persulfate as an oxidant/initiator in conjunction with aniline polymerization in concentrated hydrochloric acid to produce an acidic medium. A standard procedure was followed in preparing an aqueous solution of aniline (1 M) and HCl (0.1 M) in a beaker. After being stirred, the reaction mixture was cooled to a temperature between 0–5 °C for approximately 15 minutes. An ammonium persulfate solution (0.1 g in 5 mL distilled water) acting as an oxidant was gradually added to the aforementioned reaction mixture while being continuously stirred. The reaction mixture was stirred for 2 hours until a solid precipitate formed and then it was left overnight to set, under static conditions for 12 h at 0–5 °C. The polymer (PANI) drops to the bottom due to its high molecular weight, while unreacted aniline and oligomer remain in the supernatant and are removed. After separation, 10 mL distilled water was added and incubated for 2 hours. To remove aniline and oligomers, the process was repeated twice and the supernatant was discarded. And then distilled water was used to wash the precipitate after it had been obtained by filtering. The sample was obtained by drying it in an oven set at 60 °C for 12 hours.[19]

2.3 Synthesis of a PANI@Cu nanocomposite

The aniline hydrochloride solution was prepared by dissolving 1 M aniline monomer in 0.1 M HCl to produce an acidic medium. Another beaker was taken and 0.015 M of copper acetate was mixed with distilled water to form a solution and
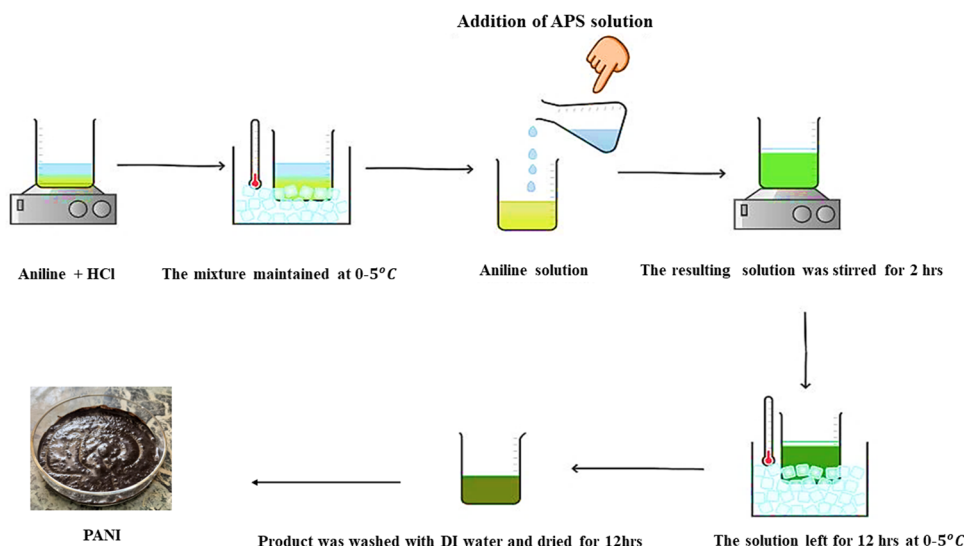
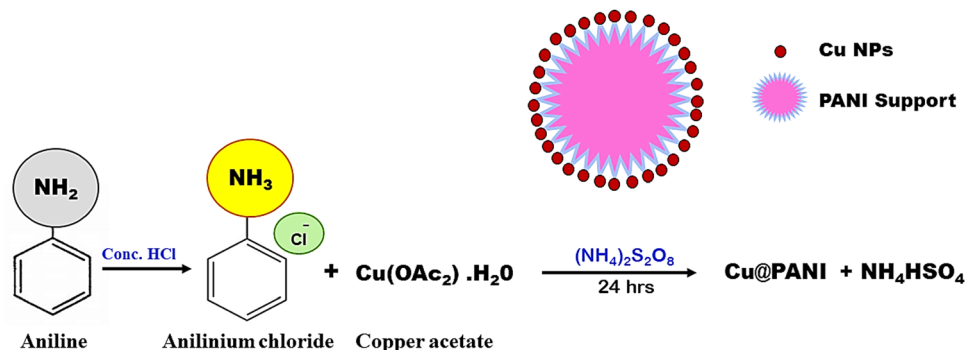**Scheme 1** Aniline and ammonium persulfate are used in the synthesis of PANI in acidic medium.

Fig. 1 Methods for the preparation of the PANI@Cu nanocomposite.

Table 1 PANI with various concentrations of copper acetate

Sample	PANI (mL)	Cu (g)
PANI	10	0
PANI@Cu1	10	0.2
PANI@Cu2	10	0.5
PANI@Cu3	10	1
PANI@Cu4	10	1.5
PANI@Cu5	10	2

here, copper ions will be produced. Immediately, the copper acetate solution was added to the aniline solution while stirring with a magnetic stirrer operated at 600 rpm. After gently adding copper ion-containing aniline to the solution, an oxidant solution of ammonium persulfate (0.1 g in 5 mL distilled water) was added to the reaction mixture. Simultaneously, this started the polymerization of aniline and the reduction of copper ions, and over time, the solution becomes darkened as a result of the formation of the PANI@Cu nanocomposite. The reaction was allowed to continue for a particular duration, typically hours, in order to allow full polymerization and reduction of copper ions. Once the reaction was finished, distilled water was used to wash the precipitate after it had been obtained by filtering. The sample was obtained by drying it in an oven set at 60 °C. A PANI@Cu nanocomposite may be synthesized according to the steps shown in Fig. 1. PANI@Cu nanocomposites were prepared with different concentrations of copper acetate (0.015, 0.03, 0.06, 0.09 and 0.12 M), hereafter called PANI@Cu1, PANI@Cu2, PANI@Cu3, PANI@Cu4 and PANI@Cu5, respectively, as shown in Table 1.

2.4 Preparation of gas concentrations, sensing response and sensitivity

The gas response was measured using a 900 cm^3 gas chamber that had been specifically prepared. We used a static mode to detect gas levels. In the gas chamber, the artificial sensor was placed. In Fig. 2 we can see a simplified representation of a gas sensing device. Using a syringe, the specified amount of test gas was delivered into the chamber until the gas concentration (in parts per million) was achieved. A scientific programmable digital sourcemeter was used to test the electrical resistance

and connected to a computer for data collection. After reaching the steady state, the sensor was exposed to fresh air to record its recovery. The chamber's input and outflow valves, labelled V_1 and V_2, were opened simultaneously to achieve this. The hoover pump was turned on simultaneously and the gas may leave the chamber through the outlet valve (V_2) and fresh air might enter through the inlet valve (V_1). The degassing process was expedited by the vacuum pump and everything was done at room temperature for measuring gas sensitivity. The required concentration of the gas is prepared by the static gas distribution method given by the formula[20,21]

$$C \text{ (ppm)} = \frac{22.4\rho TV'}{273MV} \times 1000 \qquad (1)$$

where C (ppm) is the desired target gas concentration, ρ is (g mL^{-1}) the density of the liquid (gas), V' is the volume of gas, T is the temperature in Kelvin, M is the molecular weight of gas (g mol^{-1}), and V is the volume of the chamber (L). The humidity present inside the chamber and temperature reading on the day of the experiment was 40% and $\sim$26 °C, respectively. The performance of the sensor response was evaluated using:[22,23]

$$R\% = \frac{R_a - R_g}{R_g} \qquad (2)$$

In this case, R_a represents the air standby resistance and R_g the resistance after being exposed to a reducing gas. The sensor is able to respond to NH$_3$ gas by modulating the response/recovery time between different concentrations of metal doped and various amounts of NH$_3$ gas. According to the IUPAC, sensitivity is defined as the slope of the calibration curve (sensing response versus target gas concentration):

$$S = \Delta R/\Delta C \qquad (3)$$

here ΔR and ΔC are the change in sensor response and concentration.

3. Results and discussion

3.1 X-Ray diffraction

In addition to providing information on the size of the particles, XRD spectra also offer insights into the crystallinity, lattice
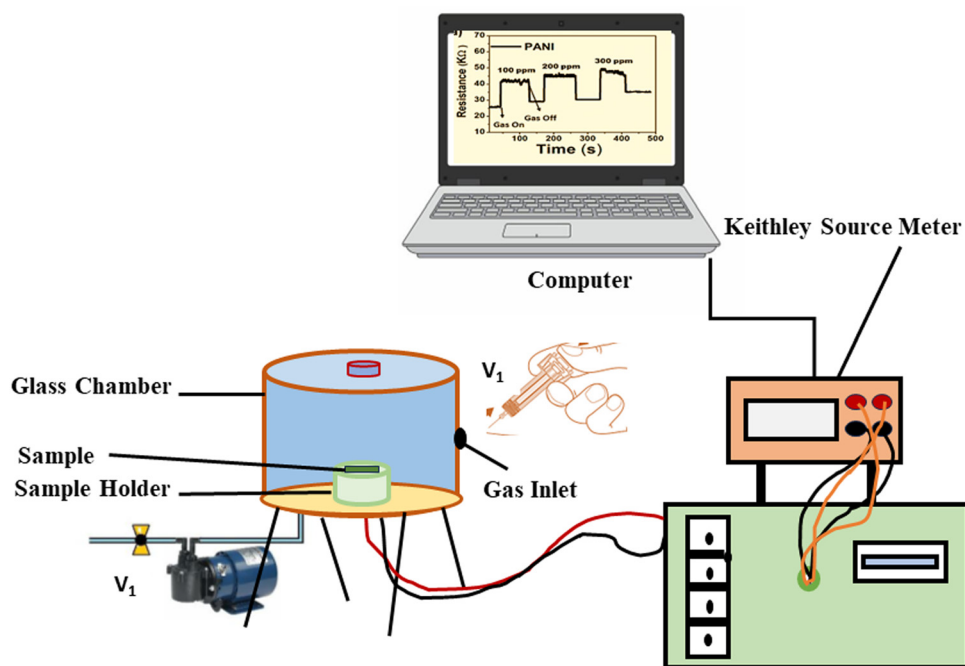
Fig. 2 Schematic diagram of a gas sensing experimental setup.

constant, and *d*-spacing of the compounds, among other structural characteristics. Fig. 3a and b illustrate the XRD spectra of pure PANI and PANI@Cu. The diffraction patterns of PANI reveal the presence of both crystalline and amorphous components, as evidenced by the peaks at 2θ of approximately $11.66°$, $18.38°$, $20.43°$, and $25.55°$. Similar to the findings of Bhagwat

et al.,[24] the crystalline PANI is attributed to the planar character of the benzenoid and quinoid functional groups, as well as the nanofiber structure. The polymer chain parallel periodicity correlates to the peak at $20.43°$, whereas the monoclinic periodicity can be related to the peak at $26.36°$. In the XRD pattern of the PANI@Cu nanocomposite, in addition to the PANI broad
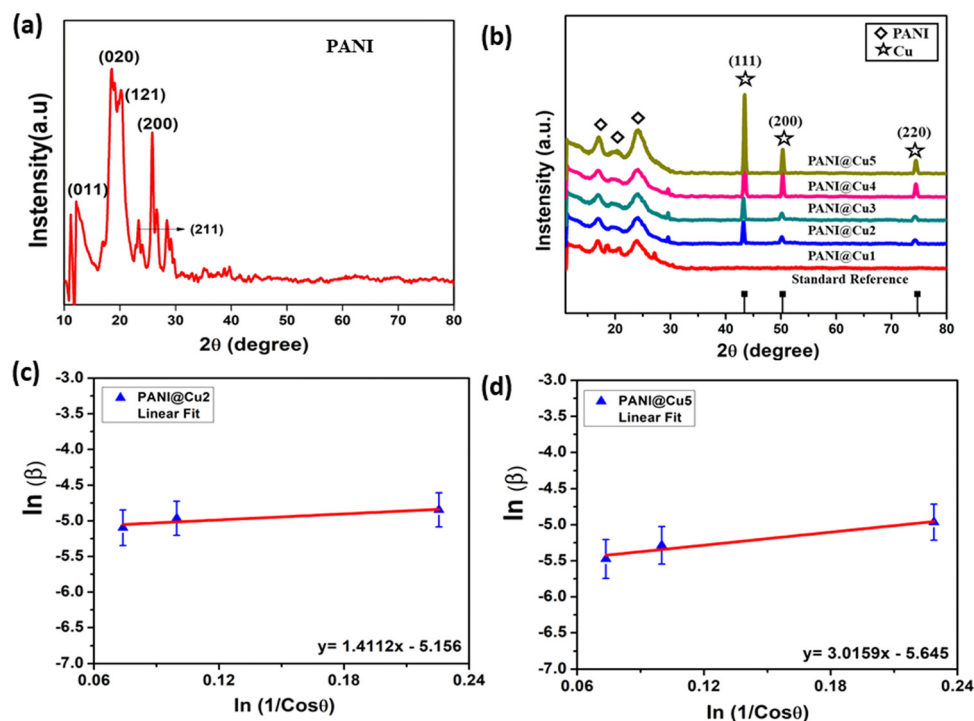

Fig. 3 XRD spectra of (a) PANI and (b) the PANI@Cu nanocomposite, and (c) and (d) Williamson−Hall plot of the nanocrystalline copper sample.

Table 2 The crystallite size of the PANI@Cu nanocomposite

Conc. (g)	2θ of the intense peak (degree)	hkl	FWHM of intense peak (β) radians	Size of the particle (D) nm	d-Spacing nm	Lattice parameter (a) Å	Macrostrain ($\varepsilon \times 10^{-3}$)	Dislocation density ($\delta \times 10^{-3}$/nm^2)
0.5	43.50	111	0.0061	12.2	2.07	3.60	3.82	1.67
1	43.31	111	0.0055	13.3	2.08	3.51	3.51	1.48
1.5	43.41	111	0.0045	16.4	2.08	3.60	2.85	0.92
2	43.42	111	0.0041	17.8	2.08	3.60	2.63	0.78

peak, three distinct diffraction peaks can be seen with maximum intensity at approximately 43°, 50° and 74°. These peaks correspond to Bragg reflections from the (111), (200), and (220) planes of Cu nanoparticles, and their intensities align with the values found in the literature (JCPDS no. 04-0836),[25] indicating that the PANI@Cu nanocomposites contain face-cantered cubic lattice Cu. In the Williamson–Hall plot as shown Fig. 3c and d in order to ascertain the strain as well as particle size, the intercept point on the Y-axis and the slope, respectively, are calculated by fitting the given plot. Despite the model's inability to take into consideration the fact that crystals display spatial variation, the current study used a Williamson–Hall analysis of nanocomposite Cu in a PANI matrix assuming uniform deformation. Fig. 3b depicts our model for Cu nanoparticle system uniform displacement. In nanocomposites the size of the Cu phase crystals is determined by applying Scherrer's formula, which corresponds to a peak at $2\theta = 43°$ with $D = 0.9\lambda/\beta\cos\theta$, where λ is the wavelength of the X-rays and β is the full width at half maximum (FWHM).[26,27] The average size range for Cu phase crystallites is 14 nm.[28] Table 2 indicates that increasing copper concentration results in an increase in particle size and d-spacing, reflecting the intricate interplay between nucleation, growth, and crystal structure in the material system being studied.

3.2 FT-IR study

FTIR was then used to explore the interaction between Cu and PANI, as shown in Fig. 4. The peak at 1460 cm^{-1} corresponds to the C=C stretching vibration of a quinoid,[29] while the peaks at 1303, 1137, and 810 cm^{-1} correspond to the C=C extension vibration mode of benzenoid rings, the stretching mode of N=Q=N (Q belongs to the quinoid ring), and the C–H bonding mode of aromatic rings, respectively.[30] All samples show substantial absorption bands in the 720–1595 cm^{-1} range, indicating PANI features. The absorbance peak at around 750 cm^{-1} corresponds to the C–H out-of-plane bending vibration of the 1,4-distributed benzene ring.[31] In the PANI, a strong absorption intensity band at ~868 cm^{-1} is assigned to the C–H out of plane bending vibration of the benzene ring deformation[32]. The benzenoid C–N[33] is responsible for the 1303 cm^{-1} band, while N–H stretching of secondary amines[34] causes the peak at 3446 cm^{-1}. These results confirmed that the Cu@PANI nanocomposite could be successfully obtained. Compared to PANI, the peak at 1561 cm^{-1} is somewhat red-shifted, while the peaks at 1302 and 1458 cm^{-1} have weakened. This is due to the π–π interaction between the Cu nanoparticles in the PANI matrix.
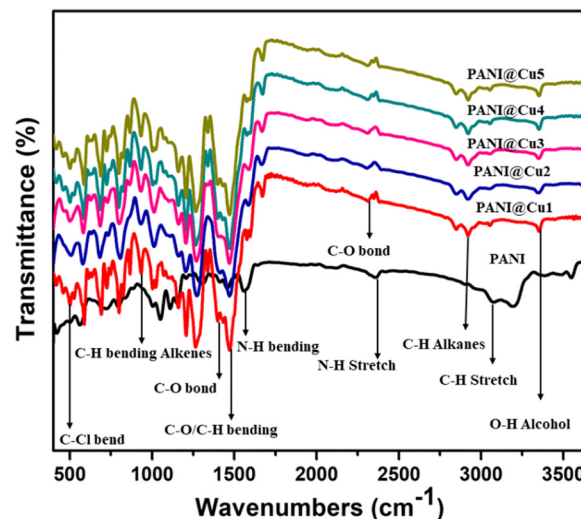

Fig. 4 FT-IR spectra of PANI and the PANI@Cu nanocomposite.

Table 3 displays the appropriate peak positions from the infrared spectra of the PANI and PANI@Cu nanocomposites.

3.3 Optical analysis and band gap values

One significant component of expanding the applications of PANI and PANI@Cu nanocomposites is the investigation of their optical characteristics. In the UV-vis spectra of PANI (Fig. 5a), the π–π* transition and the polaron band transitions are indicated by two absorption peaks at 255 and 294 nm. It seems that an excitonic transition in the quinoid ring causes another strong absorption shoulder at approximately 412 nm.[35] On the other hand, the PANI@Cu1 to PANI@Cu5 (Fig. 5b)

Table 3 The FTIR analysis of the PANI and PANI@Cu nanocomposite

Assignment	Band position (cm^{-1})	
	PANI	PANI@Cu
Stretching vibrations of –OH groups	3547	3553
C–H stretching vibrations (alkanes)	3074	2922
C–O bond	—	2350
N–H bending vibrations of amino groups	1561	1575
C=C stretching vibrations of quinoid ring	1458	—
C=C vibration of benzenoid rings	1302	1303
C–O primary/secondary alcohol	—	1207
C–H bending alkenes	1157	1160
C–O stretching vibrations/alkyl ammine	1047	1027
Chloride group incorporation in the polymer chain	573	501

nanocomposites all exhibited three absorption peaks at different wavelengths: 233, 316 and 434 nm; 230, 315 and 433 nm; 218, 314 and 429 nm; 227, 317 and 430 nm; and 221, 318, and 431 nm, respectively, in their spectra. At approximately 430 nm, an electron and polaron transition from the benzenoid ring to the quinonoid ring is attributed to the absorption peak. The PANI@Cu nanocomposite exhibited a considerably greater capacity for light absorption than pure PANI nanoparticles.[20] Crucially as previously described by C. Burda *et al.*[36] and S. Linic *et al.*[37] the PANI@Cu1 nanocomposites exhibited a peak at 434 nm, which corresponds to the surface plasmon resonance of the implanted copper nanoparticles in the polymer matrix. The band in the visible region is also defined, which means that the absorbance in the visible region is higher as a result of the Cu nanoparticle behaviours. According to the Tauc equation $\alpha = (h - E_g)^2 / h\nu$, the optical band gap of powder samples can be approximated using the direct allowed transition type, where E_g is the optical band gap, h is the Planck constant, and ν is the reciprocal of the wavelength with α as the absorption coefficient.[38,39] The spectrum analysis yielded transition bandgaps (E_g) of approximately 2.21 eV for pure PANI, 2.46 eV for PANI@Cu1, 2.47 eV for PANI@Cu2, 2.48 eV for PANI@Cu3, 2.49 eV for PANI@Cu4 and 2.49 eV for the PANI@Cu5 nanocomposite, as shown in Fig. 5c. Charge neutrality, the introduction of dopant energy levels, coulombic interactions and quantum confinement effects are all variables that alter the material electronic structure, which causes the band gap to widen as the copper concentration increases in the PANI matrix.

3.4 Morphological analysis

Images from field emission scanning electron microscopy (FESEM) of PANI, and the PANI@Cu1 and PANI@Cu5 nanocomposites are presented in Fig. 6, in that sequence. Fig. 6a and d show that PANI is characterized by nanofibrous agglomeration of inhomogeneous-shaped particles with widths of around 100 nm and lengths varying from hundreds of nanometres to several micrometres. Clusters of unevenly sized particles in the nanofibers are formed when aniline oligomer self-assembly occurs due to π–π contact, hydrogen bonding, and van der Waals forces, according to the research of Sheng Du *et al.*[40] When comparing the PANI@Cu (Fig. 6b and c)

nanocomposite samples, it is clear that the former exhibits heterogonous nucleation-induced aggregation in the form of huge globules. The fact that there are no holes in the structure proves that the particles truly do interact with one other. The FE-SEM micrographs of the composite samples show that the nano-scaled particles are evenly distributed throughout the polymer matrix. This could be because the grass particles are chemically bound to the polymer and the polymer is preventing the undesirable grass particles from obstructing the narrower particle dispersion.[41] High surface area to volume ratio Cu nanoparticles improve their gas detecting properties, therefore enabling more effective sensor designs and improved sensitivity and reactivity. Furthermore, the nonporous nanofibers have a much higher surface area; so, the homogeneous coating of Cu nanoparticles with PANI chains reduces as the Cu content in the composite rises. Particles might group or come together to create more complex forms. More metal atoms from higher metal concentrations help to increase particle–particle interactions, hence promoting aggregation. On the other hand, very high concentrations could cause particle crowding, therefore restricting their capacity for aggregation and hence producing lower individual particle sizes. Many times, nanofibers and other materials feature related vacant areas or channels. These pathways allow gas molecules to permeate through the material, facilitating quick and efficient gas interaction with the sensor devices.[42,43] Because of this, it can respond faster and identify gases more accurately.

3.5 Dispersive X-ray spectroscopy (EDX)

Sample elements are revealed by EDS. The sample elemental composition is ascertained by analysing its characteristic dispersive X-rays. As seen in Fig. 6, the EDS analysis returns the following results. The presence of carbon, nitrogen, and oxygen would be most prominently exhibited in an EDS analysis of pure polyaniline. These components make up the backbone of the polymer, as illustrated in Fig. 7a. It is clear from the pictures that copper ions can get through the PANI matrix (see Fig. 7b). Visual inspection confirmed the presence of Cu, N, and C in the PANI@Cu5 blend. Since the H signal has a lower energy, it is not present.[44] More elements, namely Cl and O, came into being as a result of the addition of HCl and ammonium persulfate solution. Thus, the surface plays a
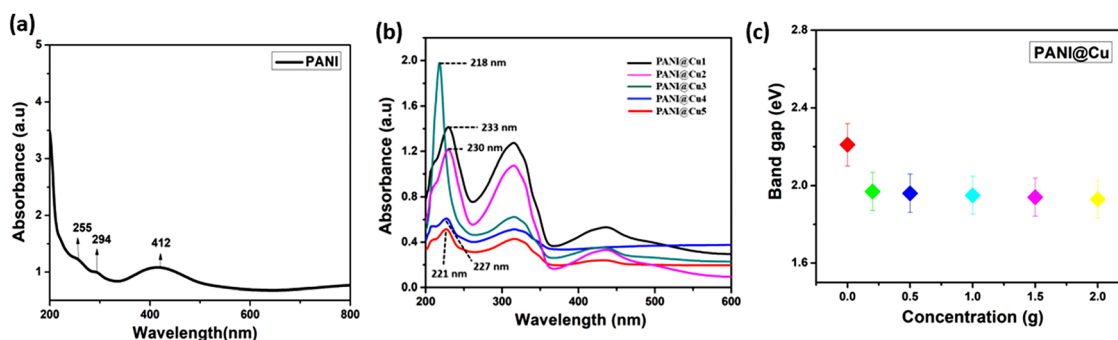

Fig. 5 UV spectrum of (a) pure PANI and (b) the PANI@Cu nanocomposite, (c) the band gap of PANI and PANI@Cu1–5 with various concentrations.
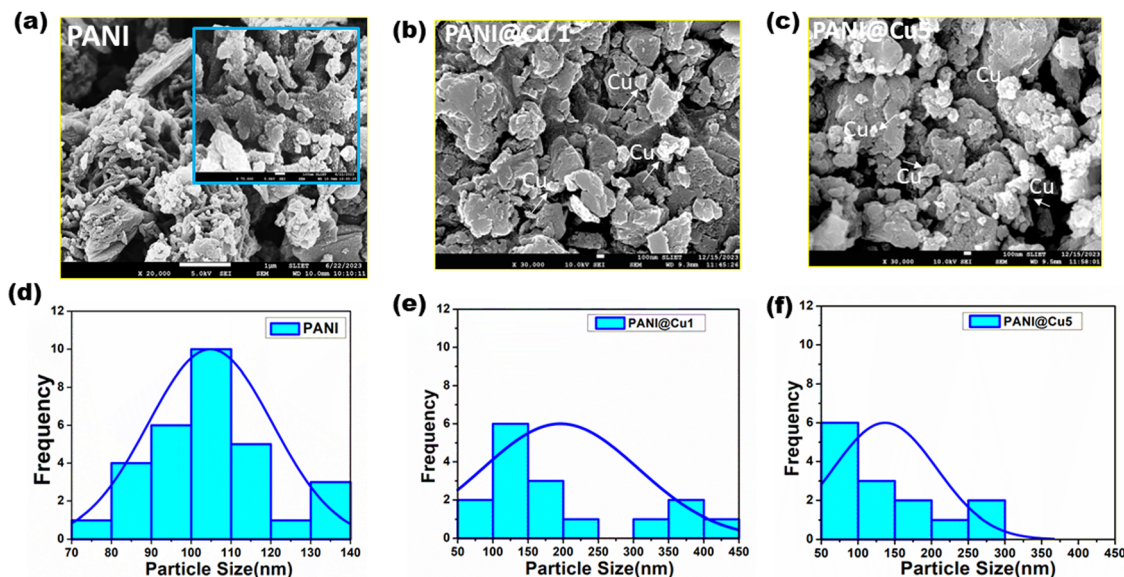
Fig. 6 FE-SEM of (a) PANI and (b) and (c) the PANI@Cu nanocomposites, and (d)–(f) particle size analysis of the samples.
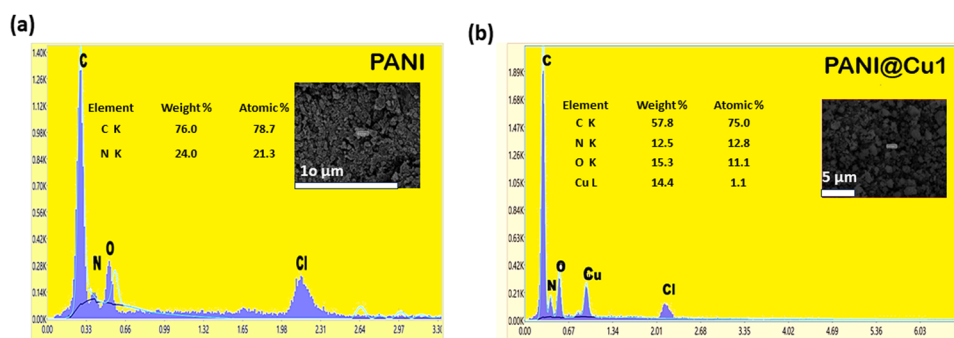

Fig. 7 (a) EDX spectra of PANI and (b) the PANI@Cu nanocomposite.

pivotal role in gas sensing, and the characteristics of the fibre samples are highly advantageous for these applications.

3.6 Thermogravimetric (TG) and differential thermal analysis (DTA)

The thermal stability of the synthesized PANI and typical PANI@Cu1 composites was investigated using a 100 °C min^{-1} heating rate and a dynamic nitrogen flow, in conjunction with TGA and DTA studies. Fig. 8a and b show pure PANI as a result of the TGA/DTA trace and adsorbed water molecules desorb at 100 °C, with the sample losing 5.53% of its weight between room temperature and that temperature. An endothermic peak at 156 °C was observed on the DTA trace, indicating this desorption. There is no noticeable effect on weight loss between 100 °C and 203 °C. Here, we can see that the material can resist quite high temperatures. The DTA trace then showed a big endothermic peak at 299 °C and a constant loss of mass from 203 °C to 638 °C. A staggering 42.46% was lost. This mass loss occurs when the polymer burns. Chemically oxidized PANI

is also compatible with it, according to the temperature data from this study.[45] When PANI samples are produced by chemical oxidation pathways, they exhibit an uneven loss of weight and do not contain a distinct dehydration step. The interfacial polymer method includes a clear dehydration step and a steady weight loss for breakdown, making it a potential candidate for synthesising substituted PANI for targeted uses. Degradation of the PANI@Cu2 nanocomposites is two-stage as shown Fig. 8c and d by the TGA-DTA results: (a) the first weight loss of 4.23% was likely associated with planar water loss; (b) the subsequent weight loss of 46.6% was caused by polymeric chain degradation and the polyaniline benzene ring-opening breakdown.[46] At the temperatures used to measure thermal conductivity, the PANI@Cu2 nanocomposite showed remarkable stability, according to the TGA data.

3.7 Gas sensing studies

3.7.1 The preparation of PANI film. A viscous solution was prepared by dissolving the pure polyaniline in *N*-methyl
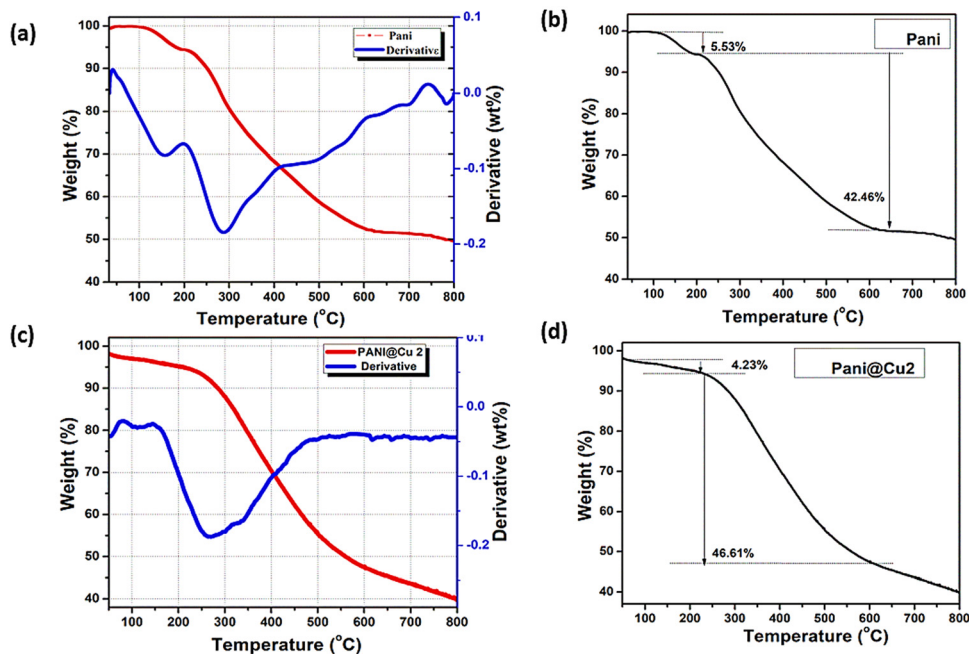
Fig. 8 TG/DTA curves of (a) and (b) traces of pure PANI and (c) and (d) the PANI@Cu nanocomposite.

pyrrolidone (NMP). This solution was used to deposit the PANI layer on a silicon substrate using the spin coating method. The process was carried out at 1500 rpm for 20 seconds. Additionally, silver paste was used to create electrical connections on the PANI film. The width of the track and the gaps between two successive tracks were 1 mm each.

3.7.2 The preparation of the PANI@Cu nanocomposite film. The prepared sample of the PANI@Cu nanocomposite film (2 mg) was dissolved in 0.1 M polyvinyl pyrrolidone to make a solution. The spin coating process was employed to deposit a layer of PANI@Cu nanocomposite on a silicon substrate using this solution. For 10 seconds, the procedure was run at 1500 rpm. In addition, the manufactured nanocomposite film was electrically connected using silver paste.

3.7.3 Gas response. Fig. 8 shows the results of the study, which included monitoring the fluctuation in resistance over time at room temperature. According to the data, films that are exposed to NH_3 gas have an increased resistance, which diminishes as the gas is closed.[47] Fig. 9a illustrates the detection range for ammonia, which is between 100 and 300 ppm, as a function of the sensor resistance. In spite of being subjected to varying amounts of NH_3 gas, the resistance value of the pure PANI-based sensor does not change significantly. Simultaneously, the resistance values of sensors built of PANI@Cu nanocomposite films with different concentrations of doped metal experienced a significant decrease in the resistance compared to PANI. The resistance values revert to their approximate baseline levels after each reaction and recovery time, which occurs when the test chamber is filled with air. To be more specific, the resistance of the PANI@Cu nanocomposite sensors ranges from 16 kΩ to 48.5 kΩ for the PANI@Cu1 nanocomposite film, from 15.7 kΩ to 46.1 kΩ for the

PANI@Cu2 nanocomposite film, from 18.7 kΩ to 43.1 kΩ for the PANI@Cu3 nanocomposite film, from 18.7 kΩ to 48.1 kΩ for the PANI@Cu4 nanocomposite film, 19.3 kΩ to 49.4 kΩ for the PANI@Cu5 nanocomposite film, and from 25.2 kΩ to 47.3 kΩ for the pure PANI sensor, as shown in Fig. 9a. The responsiveness of the composite conducting polymer sensor to NH_3 vapours is depicted in Fig. 9b. For the purpose of illustrating how the gas sensor reacts to different concentrations, we developed a graph visual. At a concentration of 300 ppm, the bar chart makes it abundantly evident that the PANI film reacts 50% and PANI@Cu5 reacts 62% towards NH_3 gas. This demonstrates that the PANI@Cu nanocomposite film sensor is suited for real-time gas sensor design for the detection of NH_3 gas under ambient conditions due to the fact that it has an outstanding selectivity for this gas. Using the data in Fig. 9b and the response values displayed in Table 4, we can see how the sensors assembled for this work react to different amounts of ammonia gas. For example, at a concentration of 100 ppm of NH_3 gas, sensors based on PANI@Cu1, PANI@Cu2, PANI@Cu3, PANI@Cu4, and PANI@Cu5 nanocomposite films exhibit 51%, 53%, 55%, 54%, and 59% improvement over sensors based on pure PANI, respectively. There are potential synergistic effects that improve the sensing performance when Cu and PANI are combined. Cu has the ability to modify PANI's electronic structure, which in turn enhances the mobility of charge carriers and their interaction with gas molecules. A more sensitive and responsive sensor may be the outcome of the synergy between Cu and PANI. In comparison to a pure PANI sensor, the PANI@Cu nanocomposite film exhibits a significantly more favourable response to NH_3 gas, according to these results. Over the course of seven days, we monitored the sensor reactions after exposure to a 100 ppm NH_3 gas alternative in
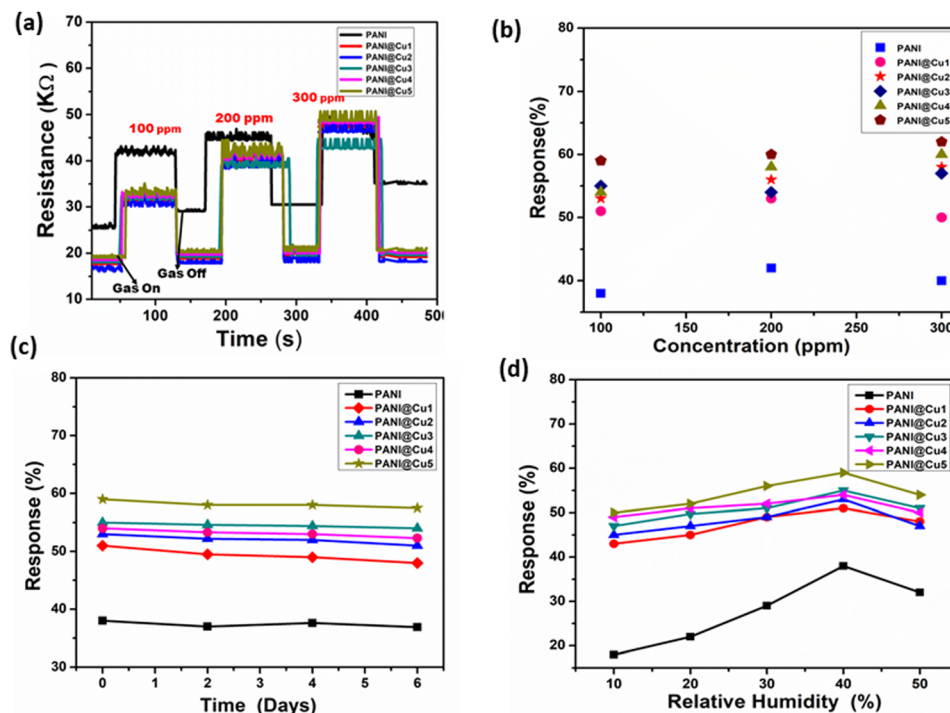
Fig. 9 (a) The shift in resistance for the pure PANI film and different concentrations of Cu nanoparticles (PANI@Cu1 to PANI@Cu5 nanocomposite) relative to time when exposed to NH$_3$ gas at room temperature, (b) the sensing response of PANI and PANI@Cu1 to the PANI@Cu5 nanocomposite film with varying NH$_3$ concentrations, (c) stability of the gas sensor based on PANI and the PANI@Cu1 to PANI@Cu5 nanocomposite film toward 100 ppm ammonia and (d) effect of humidity on the prepared sensor when exposed to 100 ppm ammonia.

Table 4 The response values of sensors prepared in this work regarding NH$_3$ gas

NH$_3$ gas concentration response (%)	100 (ppm)	200 (ppm)	300 (ppm)
PANI	38	42	40
PANI@Cu1	51	53	50
PANI@Cu2	53	56	58
PANI@Cu3	55	54	57
PANI@Cu4	54	58	60
PANI@Cu5	59	60	62

order to assess the formed gas sensor initial long-term stability. Fig. 9c displays the measured sensor response ($\Delta R/R_g$) to NH$_3$ exposure for up to seven days for the PANI and PANI@Cu1 to PANI@Cu5 nanocomposite film gas sensors. After 7 days, the results show that the prepared gas sensor maintains a consistent sensing performance with just a slight decrease in response. Sensors based on PANI can be made more stable and long-lasting by using copper nanoparticles. The longevity of the sensor makes it resistant to repeated gas exposure without major degradation, and the enhanced stability makes sure that its performance remains consistent over time. In addition, we have examined the impact of humidity on the prepared PANI and PANI@Cu1–5 nanocomposite film gas sensors when exposed to 100 ppm of NH$_3$ gas in various humid environments. In Fig. 9d, we can observe the sensor reaction to varying humidity levels. Increased humidity causes the sensor to respond more strongly. At a relative humidity

(RH%) of 40%, the sensor demonstrates its highest sensing response. Thereafter, a reduction in sensor response with increasing humidity is observed. Consequently, as discussed in Section 3.8,[36–42] the conductivity changes when PANI and copper nanoparticles interact with humidity (H$_2$O) because of the complex proton exchange mechanism.

3.7.4 Response and recovery time. The subsequent crucial elements that should be taken into consideration are the evaluation of a sensor reaction and the recovery periods. The amount of time that has passed after the intake of gas and the occurrence of a discernible change in the parameter is referred to as the response time. On the other hand, the amount of time that is necessary for the parameter to return to its initial state following the removal of gas is referred to as the recovery time. Two methods are available for determining them: first, the amount of time it takes for the sensor to reach 90% saturation of R_g from R_a during gas intake, and second, the value of R_a at 10% during gas withdrawal. Both of these methods are able to be measured. Using different quantities of NH$_3$ gas, Fig. 10 shows the reaction and recovery period of the pure PANI film (Fig. 10a) and PANI@Cu nanocomposite film (Fig. 10b–f). As the NH$_3$ concentration increases from 100 to 300 ppm, the response time for pure PANI film increases from 27 to 29 s and the recovery time decreases from 22 to 20 s. In contrast, for the Cu-doped PANI (PANI@Cu1) nanocomposite film, the response time decreases from 18 to 17 s and the recovery time increases from 17 to 20 s. Table 5 presents the response times (T_1) and
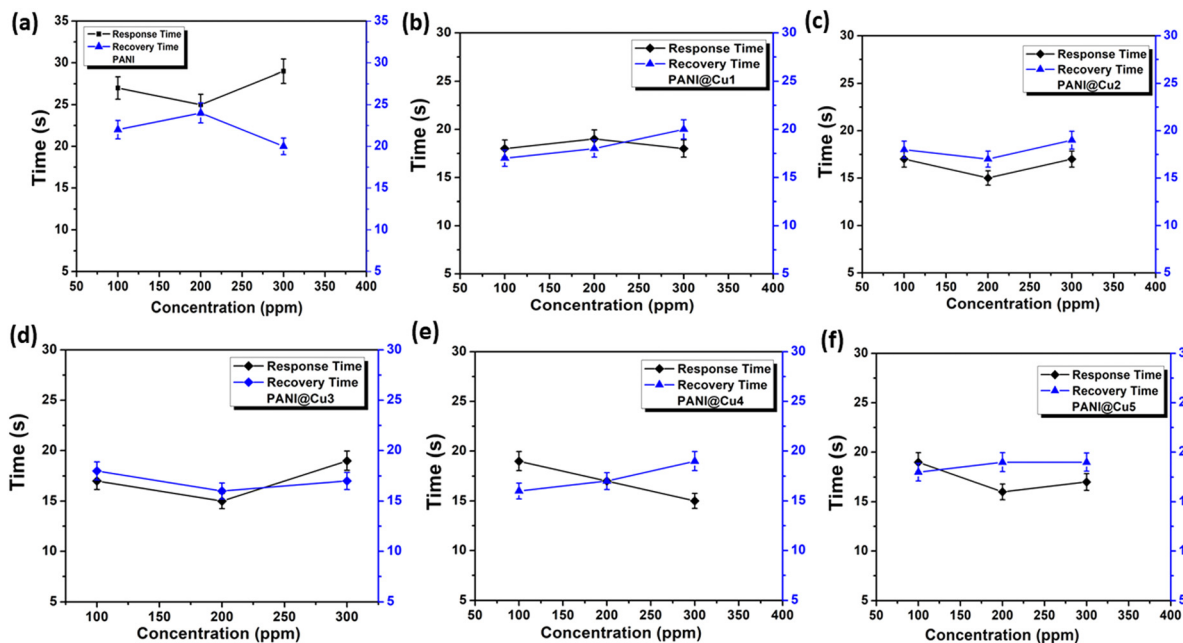
Fig. 10 Response and recovery time plot for (a) pure PANI film and (b)–(f) the PANI@Cu nanocomposite film when exposed to various concentrations of NH_3 gas at room temperature.

Table 5 Response times (T_1) and recovery times (T_2) of the sensors under 100 ppm NH_3 gas

Sensitive films	Pure PANI	PANI@Cu1	PANI@Cu2	PANI@Cu3	PANI@Cu4	PANI@Cu5
Response time (T_1)	27	18	17	18	19	19
Recovery time (T_2)	22	17	18	18	16	18

recovery times (T_2) of PANI and the PANI@Cu nanocomposite sensors after they were exposed to NH_3 gas at a concentration of 100 ppm. According to V. G. Bairi et al.[48] reduced response times are the consequence of surface roughness enhancement and beneficial dedoping brought about by the formation of a restricted polaron band when metal is present. Due to the presence of Cu ions in the PANI chain, the recovery time for the PANI@Cu3 nanocomposite film appears to be rapid. Previous tests that have been published have demonstrated response times that are significantly greater than the minimum response time of the PANI@Cu nanocomposite film, which is approximately 20 seconds. Fast oxidation of NH_3 gas could be a reason for the PANI@Cu sensor's quick response to the gas. Sensing measures in real-world contexts often necessitate a fast reaction time; yet, recovery time is little impacted even if it is crucial for the sample to return to its original state.[49] It is evident that PANI@Cu nanocomposite sensors often have lower response times than pure PANI sensors. Incorporating copper into the PANI matrix can enable the nanocomposite sensitive film to have a quicker response and recovery time. One possible explanation for the longer reaction and recovery durations is that the PANI nanofibers are coated and deposited on the copper during chemical polymerization, leading to a more uniform distribution and a larger surface area. Part 3.4 details how to assess this by integrating morphology and microstructure studies of the PANI@Cu nanocomposite film. A faster

response and recovery rate with less recovery time is achieved by providing more active sites for the adsorption of NH_3 gas molecules. As a result, the PANI@Cu nanocomposite film sensor is ideal for practical applications that require rapid and reliable ammonia detection under room temperature conditions. Table 6 provides a summary of the NH_3 gas-sensitive properties of the PANI@Cu nanocomposite sensor that was used in this study. These qualities are compared to those of some others that have been reported in recent times.

3.7.5 Selectivity. In this work, selectivity tests were carried out for the PANI film and PANI@Cu nanocomposite films. Fig. 11b shows the sensor response of the PANI@Cu1 nanocomposite sensor to 100 ppm concentrations of NH_3 gas, ethanol (C_2H_5OH), carbon monoxide (CO), hydrogen sulphide (H_2S) and carbon dioxide (CO_2), respectively. It is clear that the response of the PANI@Cu sensor toward NH_3 gas is significantly higher than that of the other gases measured. By combining PANI with copper nanoparticles, a synergistic effect can be achieved, where the combined qualities of both components improve the nanocomposite performance. A composite can be made more stable and conductive with the inclusion of PANI and ammonia can be adsorbed more effectively with the help of copper nanoparticles. The chemical affinity, high surface area, presence of copper nanoparticles, conductivity changes upon exposure to ammonia, and selective detection mechanisms of the PANI@Cu1 nanocomposite contribute to its

Table 6 Comparison of the PANI@Cu nanocomposite film-based gas sensor and those reported in the literature

Material	Substrate	Temp.	Gas	ppm	Response (%)	T_1 (s)	T_2 (s)	Ref.
PAN1	PET	RT	NH_3	100	26	33	—	50
PANI	Glass	RT	NH_3	10	22	—	—	51
PANI/graphene		25 °C		20	3.65	50	23	52
PANI@CuO	Glass	RT	NH_3	100	—	80	496	41
PANI/graphene		RT		20	0.6	—	—	53
Cu-en@PANI	Glass	RT	NH_3	100	3.8^a	100	—	13
PANI–CeO$_2$	PET	RT	NH_3	16 ppb	2.4^a	6 min		54
Pd/PANI	IDE	RT	NH_3	100	∼10	—		55
Au/PANI	—	RT	NH_3	100	∼3	5	7	56
CuO/PANI	PET	RT	NH_3	100	0.98^a	5.7	—	57
Ag/PANI	PET	Rt	NH_3	10	9.1			58
Pd/PANI	—	RT	NH_3	500	21.9	—		55
Cu@PANI	Glass	RT	NH_3	50	0.55^b	7	—	59
PANI	Si	RT	NH_3	100	38	27	22	This work
				200	42	25	24	
				300	40	29	20	
PANI@Cu1	Si	RT	NH_3	100	51	18	17	This work
				200	53	19	18	
				300	50	17	20	
PANI@Cu2	Si	RT	NH_3	100	53	17	18	This work
				200	56	15	17	
				300	58	16	19	
PANI@Cu3	Si	RT	NH_3	100	55	17	18	This work
				200	54	15	16	
				300	57	19	17	
PANI@Cu4	Si	RT	NH_3	100	54	19	16	This work
				200	58	17	17	
				300	60	15	19	
PANI@Cu5	Si	RT	NH_3	100	59	19	18	This work
				200	60	16	19	
				300	62	17	19	

^{a} $(R_g - R_a)/R_a$. ^{b} $(I_a - I_g)/I_a$.

good selectivity towards ammonia gas. The nanocomposite selectivity for ammonia gas detection and sensing is due, in part, to these components. There is a clear difference between ammonia and other gases in terms of its sensor response. Being highly polar and capable of hydrogen bonding, it has the potential to interact strongly with the composite film in comparison to other gases.

3.8 Sensing mechanism

A decrease in free charge carriers, which are partially consumed during complex formation as a result of an interaction between the PANI film and NH_3, an acceptor and a donor, respectively, are responsible for the rise in film resistance that occurs when the amount of NH_3 that is consumed is increased.[44] In order to counteract the rising concentration of NH_3 gas, the system must move in the direction that is prescribed by the Le Chatelier primary equilibrium. The elimination of ammonia, on the other hand, results in a different direction of balance within the system. When it comes to NH_3 gas, the electronegative charge of nitrogen is dominant over that of hydrogen. In the presence of PANI-based molecules, ammonia (NH_3) is able to create a partial polar bond with hydrogen atoms. As a result, the final product will have a greater degree of interchain separation in the PANI film. This results in a decrease in the
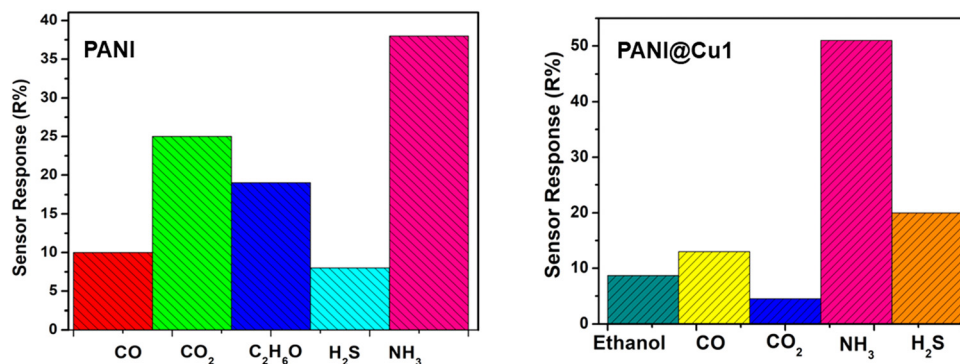

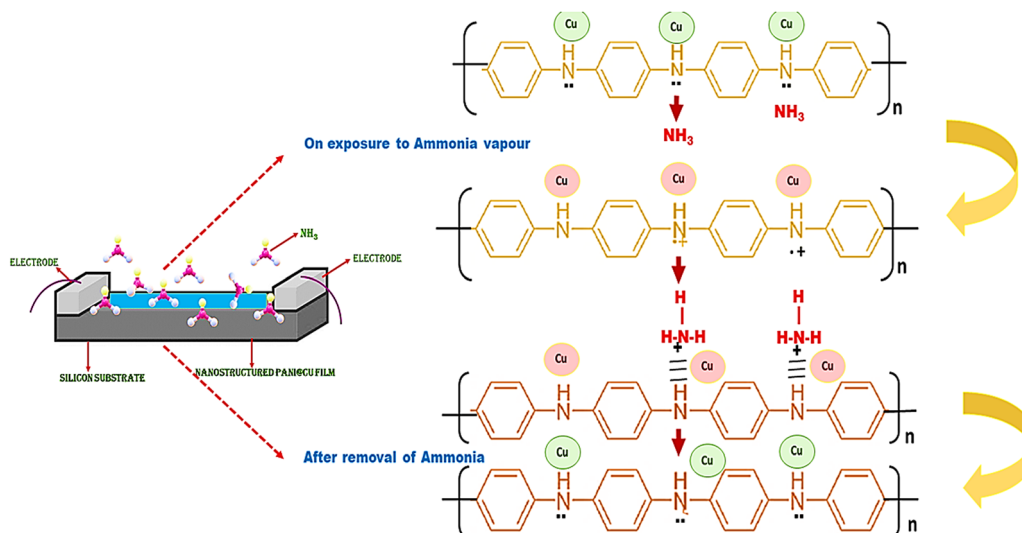**Fig. 11** Selectivity of (a) PANI and (b) the PANI@Cu1 nanocomposite film gas sensor.

Fig. 12 Schematic of the ammonia sensing mechanism.

likelihood of electron hopping, which is the fundamental conduction mechanism in PANI systems, occurring between neighbouring chains, which ultimately leads to an increase in the film resistance. It is possible for the PANI emeraldine salt to be transformed into the PANI emeraldine base form when the concentration of ammonia vapour is at its greatest.[60] Changing the emeraldine base back into emeraldine salt once the ammonia vapour has been removed is all that is required to bring the sensor functionality back to its original state. In order to perform the sensing mechanism, ammonia molecules make chemical contact with the surface of the PANI@Cu nanocomposite film. There is a possibility that, between the ammonia molecules and the copper nanoparticles, hydrogen bonds, dipole–dipole interactions, or weak chemical bonds could result. Because of these interactions, the composite material electrical properties, such as its conductivity and other quantifiable characteristics, are susceptible to change. Fig. 12 provides a schematic representation of the PANI film and PANI@Cu nanocomposite film for ammonia detection.

4. Conclusions

We have synthesized polyaniline and a polyaniline–copper (PANI@Cu) nanocomposite by a chemical oxidative polymerization method. The formation of copper nanoparticles and their presence in the prepared nanocomposite were confirmed by XRD, FTIR, FE-SEM, UV-Vis spectroscopy, TGA and EDS. The XRD patterns indicated that the crystalline phase of Cu nanoparticles is cubic with a crystallite size of 14 nm. FE-SEM analysis showed uniform dispersion of copper nanoparticle clusters in the PANI matrix. The optical studies indicated that the absorption mechanism is due to direct allowed transition and the optical band gap of polyaniline is less than that of the PANI@Cu nanocomposite. Comparing the nanocomposite to the naked PANI film, the TGA and DTG curves reveal that the

latter is relatively unstable. Copper nanoparticle intercalated PANI nanocomposite films were tested at room temperature for their gas sensing capabilities with respect to NH_3, CO, CO_2, H_2S, and ethanol. At ambient temperature, the nanocomposite films showed improved response kinetics and a highly selective response toward NH_3. For instance, among all of the materials evaluated, the sensor film with 2 g of Cu nanoparticles (PANI@Cu5) had the best sensor response (62%), with response and recovery times of 19 and 18 s, respectively, towards 300 ppm of NH_3. The greater response might be because the copper nanoparticle intercalation in the PANI matrix increased the surface area and improved the charge transfer. Therefore, nanocomposite film sensors show promise in the gas-sensor industry due to their rapid reaction time, reasonable selectivity towards ammonia, and somewhat stable operation at room temperature. In conclusion, we assert that the addition of copper to PANI has resulted in a much-enhanced ammonia sensor.

Data availability

The data used to support the Findings of this study are available from the corresponding author upon request.

Conflicts of interest

There are no conflicts to declare.

Acknowledgements

References

1 M. J. Palys, *et al.*, *Curr. Opin. Chem. Eng.*, 2021, **31**, 100667.

2 G. Wu, *et al.*, *Sens. Actuators, B*, 2024, **418**, 136328.

3 A. Verma and T. Kumar, PANI@Ag nanocomposites gas sensors for rapid detection of ammonia, *Polyhedron*, 2024, 116982.

4 B. Timmer, W. Olthuis and A. V. Berg, Ammonia sensors and their applications-a review, *Sens. Actuators, B*, 2005, **107**(2), 666–677.

5 Y. J. Zhang, W. Zeng and Y. Q. Li, Porous MoS$_2$ microspheres decorated with Cu$_2$O nanoparticles for ammonia sensing property, *Mater. Lett.*, 2019, **241**, 223–226.

6 B. C. Omur, Humidity effect on adsorption kinetics of ammonia onto electrospun SnO$_2$ nanofiber, *Mater. Res. Express*, 2019, **6**(4), DOI: 10.1088/2053-1591/aafa27.

7 S. K. Bhardwaj, N. Bhardwaj, M. Kukkar, A. L. Sharma, K.-H. Kim and A. Deep, Formation of high-purity indium oxide nanoparticles and their application to sensitive detection of ammonia, *Sensors*, 2015, **15**(12), 31930–31938.

8 M. Das and D. Sarkar, One-pot synthesis of zinc oxide–polyaniline nanocomposite for fabrication of efficient room temperature ammonia gas sensor, *Ceram. Int.*, 2017, **43**(14), 11123–11131.

9 A. Verma, *et al.*, Review—Recent Advances and Challenges of Conducting Polymer–Metal Nanocomposites for the Detection of Industrial Waste Gases, *ECS J. Solid State Sci. Technol.*, 2023, **12**, 047002.

10 E. Detsri and J. Popanyasak, Fabrication of silver nanoparticles/polyaniline composite thin films using layer-by-layer self-assembly technique for ammonia sensing, *Colloids Surf., A*, 2015, **467**, 57–65.

11 V. Pentyala, *et al.*, Carbon dioxide gas detection by open metal site metal organic frameworks and surface functionalized metal organic frameworks, *Sens. Actuators, B*, 2016, **225**, 363–368.

12 A. A. Sagade and R. Sharma, Copper sulphide (Cu$_x$S) as an ammonia gas sensor working at room temperature, *Sens. Actuators, B*, 2008, **133**, 135–143.

13 S. Kumar Gautam and S. Panda, Highly sensitive Cu ethylenediamine/PANI composite sensor for NH$_3$ detection at room temperature, *Talanta*, 2023, **258**, 124418.

14 K. M. Batoo, E. Ali, B. A. Hussein, A. Al-khalidi, U. S. Altimari, S. Hussain, S. Hameed Kareem, M. Kadhem Abid, A. Alawadi and A. Ihsan, The cooperative performance of iodo and copper in a Zr-based UiO-67 metal-organic framework for highly selective photocatalytic CO$_2$ reduction to methanol, *J. Mol. Struct.*, 2024, **1307**, 137927.

15 S. Sardana, H. Kaur, B. Arora, D. Kumar Aswal and A. Mahajan, *ACS Sens.*, 2022, **7**(1), 312–321.

16 C. N. Zhu, Z. J. Wang, X. P. Li, S. Y. Chen, D. Y. Zheng, C. Liu, X. J. Liu, D. B. Cheng and Z. Y. Qiao, Site-specific activation of mitochondria-targeting peptide nanomaterials for treatment of drug-resistant tumors, *ACS Appl. Nano Mater.*, 2023, **6**, 15641–15650.

17 J. Zhang, P. Guan, W. Li, Z. Shi and H. Zhai, Synthesis and characterization of a polyaniline/silver nanocomposite for the determination of formaldehyde, *Instrum. Sci. Technol.*, 2016, **44**(3), 249–258.

18 S. Bai, Y. Tian and M. Cui, *et al.*, Polyaniline@SnO$_2$ heterojunction loading on flexible PET thin film for detection of NH$_3$ at room temperature, *Sens. Actuators, B*, 2016, **226**, 540–547.

19 R. G. Bavane, M. D. Shirsat and A. M. Mahajan, *Sens. Transducers J.*, 2010, **113**(2), 63.

20 S. T. Navale, C. Liu, P. S. Gaiker, V. B. Patil, R. U. R. Sagar, B. Du, R. S. Mane and F. J. Stadler, *Sens. Actuators, B*, 2017, **245**, 524–532.

21 P. Dipak, D. C. Tiwari and A. Samadhiya, *et al.*, Synthesis of polyaniline (printable nanoink) gas sensor for the detection of ammonia gas, *J. Mater. Sci.: Mater. Electron.*, 2020, **31**, 22512–22521, DOI: 10.1007/s10854-020-04760-2.

22 D. C. Tiwari, P. Atri and R. Sharma, Sensitive detection of ammonia by reduced graphene oxide/polypyrrole nanocomposites, *Synth. Met.*, 2015, **203**, 228–234.

23 L. M. García Rojas, C. A. Huerta-Aguilar, E. Navarrete, E. Llobet and P. Thangarasu, Enhancement of the CO$_2$ Sensing/Capture through High Cationic Charge in M–ZrO$_2$ (Li$^+$, Mg^{2+}, or Co^{3+}): Experimental and Theoretical Studies, *ACS Appl. Mater. Interfaces*, 2023, **15**, 25952–25965.

24 A. D. Bhagwat, S. S. Sawant and C. M. Mahajan, Facile rapid synthesis of polyaniline (PANI) nanofibers, *J. Nano-Electron. Phys.*, 2016, **8**(1), 8–10.

25 H. Liu, T. Wang and H. Zeng, *Part. Part. Syst. Charact.*, 2015, **32**, 869–873.

26 Polyaniline: The infrared spectroscopy of conducting polymer nanotubes (IUPAC Technical Report).

27 A. E. A. Said, M. M. E-Wahab, S. A. Soliman and M. N. Goda, *Nanosci. Nanoeng.*, 2014, **2**, 17–28.

28 B. N. Meethal, R. Ramanarayanan and S. Swaminathan, *Appl. Nanosci.*, 2018, **8**, 1545–1555.

29 X. Wang, S. Feng, W. Zhao, D. Zhao and S. Chen, *New J. Chem.*, 2017, **41**, 9354–9360.

30 B. K. Sharma, A. K. Gupta, N. Khare, S. K. Dhawan and H. C. Gupta, *Synth. Met.*, 2009, **159**, 391–395.

31 M. Trchova and J. Stejskal, *Undoped Appl. Chem.*, 2011, **83**, 1803–1817.

32 S. Khasim, S. C. Raghavendra, M. Revanasiddappa and M. V. N. Ambika Prasad, *Ferroelectrics*, 2005, **325**, 111–119.

33 J. Li, T. Peng, Y. Zhang, C. Zhou and A. Zhu, *Sep. Purif. Technol.*, 2018, **201**, 120–129.

34 M. R. Nabid, M. Golbabaee, A. B. Moghaddam, R. Dinarvand and R. Sedghi, *Int. J. Electrochem. Sci.*, 2008, **3**, 1117–1126.

35 J. Bhadra, N. K. Madi, N. J. Al-Thani and M. A. Al-Maadeed, Polyaniline/polyvinyl alcohol blends: Effect of sulfonic acid dopants on microstructural, optical, thermal and electrical properties, *Synth. Met.*, 2014, **191**, 126–134.

36 C. Burda, X. Chen, R. Narayanan and M. A. El-Sayed, *Chem. Rev.*, 2005, **36**, 1025–1102.

37 S. Linic, P. Christopher and D. B. Ingram, *Nat. Mater.*, 2011, **10**, 911–921.

38 P. Chrysicopoulou, D. Davazoglou, C. Trapalis and G. Kordas, Optical properties of very thin (<100 nm) sol–gel TiO$_2$ films, *Thin Solid Films*, 1998, **323**, 188.

39 C. A. Huerta-Aguilar, Y. S. G. Gutiérrez and P. Thangarasu, Crystal plane directed interaction of TiO$_2$ [1 0 1] with AgNPs [1 1 1] silver nanoparticles enhancing solar light induced photo-catalytic oxidation of ciprofloxacin: Experimental and theoretical studies, *Chem. Eng. J.*, 2020, **394**, 124286.

40 X.-S. Du, C.-F. Zhou, G.-T. Wang and Y.-W. Mai, Novel Solid-State and Template-Free Synthesis of Branched Polyaniline Nanofibers, *Chem. Mater.*, 2008, **20**, 3806–3808.

41 S. K. Singh, R. K. Shukla, R. Kumar, U. K. Tripathi and S. K. Mishra, Investigation on PANI/CuO nanocomposites for ammonia gas, *Mater. Lett.*, 2022, **309**, 131325. sensing applications.

42 X. Liu, W. Zheng, R. Kumar, M. Kumar and J. Zhang, Conducting polymer-based nanostructures for gas sensors, *Coord. Chem. Rev.*, 2022, **462**(1), 214517.

43 J. Song, X. Lin and L. Y. Ee, *et al.*, A Review on Electrospinning as Versatile Supports for Diverse Nanofibers and Their Applications in Environmental Sensing, *Adv. Fiber Mater.*, 2023, **5**, 429–460.

44 K. Crowley, A. Morrin, A. Hernandez, E. O'Malley, P. G. Whitten, G. G. Wallace, M. R. Smyth and A. J. Killard, *Talanta*, 2008, **77**, 710–717.

45 P. K. Khanna, V. V. V. S. Subbarao, N. Singh, R. Gokhale and U. P. Mulik, Synthesis and characterization of Ag/PVA nanocomposite by chemical reduction method, *Mater. Chem. Phys.*, 2005, **93**, 117.

46 V. Tauc and A. Menth, States in the gap, *J. Non-Cryst. Solids*, 1972, **8–10**, 569–585.

47 S. Konwer, A. K. Guha and S. K. Dolui, Graphene oxide-filled conducting polyaniline composites as methanol-sensing materials, *J. Mater. Sci.*, 2013, **48**(4), 1729–1739.

48 V. G. Bairi, S. E. Bourdo, N. Sacre, D. Nair, B. C. Berry, A. S. Biris and T. Viswanathan, Ammonia gas sensing behavior of tanninsulfonic acid doped polyaniline–TiO$_2$ composite, *Sensors*, 2015, **15**, 26415–26429.

49 C. Drake, A. Amalu, J. Bernard and S. Seal, Enhancing the low temperature hydrogen sensitivity of nanocrystalline SnO$_2$ as a function of trivalent dopants, *J. Appl. Phys.*, 2007, **101**(10), 104307.

50 D. K. Bandgar, S. T. Navale, S. R. Nalage, R. S. Mane, F. J. Stadler, D. K. Aswal, S. K. Gupta and V. B. Patil, Simple and low-temperature polyaniline-based flexible ammonia sensor: a step towards laboratory synthesis to economical device design, *J. Mater. Chem.*, 2015, **3**, 9461–9468.

51 Q. X. Nie, Z. Y. Pang, D. W. Li, H. M. Zhou, F. L. Huang and Y. B. Cai, *et al.*, Facile fabrication of flexible SiO$_2$/PANI nanofibers for ammonia gas sensing at room temperature, *Colloids Surf., A*, 2018, **537**, 523–539, DOI: **10.1016/j.colsurfa.2017.10.065**.

52 Z. Wu, X. Chen and S. Zhu, *et al.*, Enhanced sensitivity of ammonia sensor using graphene/polyaniline nanocomposite, *Sens. Actuators, B*, 2013, **178**, 485–493.

53 M.-S. Kim, S. Kim and H. J. Kong, *et al.*, Tunable electrical-Sensing performance of random-alternating layered graphene/polyaniline Nanoarchitectures, *J. Phys. Chem. C*, 2016, **120**, 18289–18295.

54 C. Liu, H. Tai, P. Zhang, Z. Yuan, X. Du, G. Xie and Y. Jiang, A high-performance flexible gas sensor based on self-assembled PANI–CeO$_2$ nanocomposite thin film for trace-level NH$_3$ detection at room temperature, *Sens. Actuators, B*, 2018, **261**, 587–597.

55 H. T. Hien, H. T. Giang and N. V. Hieu, *et al.*, Elaboration of Pd-nanoparticle decorated polyaniline films for room temperature NH$_3$ gas sensors, *Sens. Actuators, B*, 2017, **249**, 348–356.

56 U. V. Patil, N. S. Ramgir and N. Karmakar, *et al.*, Room temperature ammonia sensor based on copper nanoparticle intercalated polyaniline nanocomposite thin films, *Appl. Surf. Sci.*, 2015, **339**, 69–74.

57 B. Sakthivel, L. Manjakkal and G. Nammalvar, High performance CuO nanorectanglesbased room temperature flexible NH$_3$ sensor, *IEEE Sens. J.*, 2017, **17**, 6529–6536.

58 S. Bai, C. Sun and P. Wan, *et al.*, Transparent conducting films of hierarchically nanostructured polyaniline networks on flexible substrates for high-performance gas sensors, *Small*, 2015, **11**, 306–310.

59 U. V. Patil, N. S. Ramgir, N. Karmakar, A. Bhogale, A. K. Debnath, D. K. Aswal, S. K. Gupta and D. C. Kothari, Room temperature ammonia sensor based on copper nanoparticle intercalated polyaniline nanocomposite thin films, *Appl. Surf. Sci.*, 2015, **339**, 69–74.

60 Z. Pang, Z. Yang, Y. Chen, J. Zhang, Q. Wang, F. Huang and Q. Wei, *Colloids Surf., A*, 2016, **494**, 248–255.